Effects of F^- Doping on the Photocatalytic Activity and Microstructures of Nanocrystalline TiO_2 Powders

Jimmy C. Yu,*,† Jiaguo Yu,†,‡ Wingkei Ho,† Zitao Jiang,† and Lizhi Zhang†

Department of Chemistry and Materials Science & Technology Research Centre, The Chinese University of Hong Kong, Shatin, New Territories, Hong Kong, China, and State Key Laboratory of Advanced Technology for Materials Synthesis and Processing, Wuhan University of Technology, Wuhan 430070, China

Received January 15, 2002. Revised Manuscript Received May 15, 2002

A novel and simple method for preparing highly photoactive nanocrystalline F^--doped TiO_2 photocatalyst with anatase and brookite phase was developed by hydrolysis of titanium tetraisopropoxide in a mixed NH_4F-H_2O solution. The prepared F^--doped TiO_2 powders were characterized by differential thermal analysis-thermogravimetry (DTA-TG), X-ray diffraction (XRD), X-ray photoelectron spectroscopy (XPS), UV−vis absorption spectroscopy, photoluminescence spectra (PL), transmission electron microscopy (TEM), and BET surface areas. The photocatalytic activity was evaluated by the photocatalytic oxidation of acetone in air. The results showed that the crystallinity of anatase was improved upon F^- doping. Moreover, fluoride ions not only suppressed the formation of brookite phase but also prevented phase transition of anatase to rutile. The F^--doped TiO_2 samples exhibited stronger absorption in the UV−visible range with a red shift in the band gap transition. The photocatalytic activity of F^--doped TiO_2 powders prepared by this method exceeded that of Degussa P25 when the molar ratio of NH_4F to H_2O was kept in the range of 0.5−3.

1. Introduction

A great deal of effort has been devoted in recent years to developing heterogeneous photocatalysts with high activities for environmental applications such as air purification, water disinfection, hazardous waste remediation, and water purification.[1−10] Among various oxide semiconductor photocatalysts, titania has proven to be the most suitable for widespread environmental applications for its biological and chemical inertness, strong oxidizing power, cost effectiveness, and long-term stability against photocorrosion and chemical corrosion.[1] Titania can be used to catalyze many reactions, such as alcohol dehydration, Photo-Kolbe oxidations of organic acids,[11] oxidation of aromatic compounds,[12] degradation of paint pigments,[13] and nitrogen oxide reduction[14] under UV illumination. The detailed mechanism and factors influencing its activity, however, are poorly understood.[11,15]

The photocatalytic activity of semiconductors is due to the production of excited electrons in the conduction band of the semiconductors, along with corresponding positive holes in the valence band by the absorption of UV illumination. These energetically excited species are mobile and capable of initiating many chemical reactions, usually by the production of radical species at the semiconductor surface. They are unstable, however, and recombination of the photogenerated electrons and holes can occur very quickly, dissipating the input energy as heat.[15,16] In fact, the photocatalytic efficiency depends on the competition between these two processes, that is, the ratio of the surface charge carrier transfer rate to the electron−hole recombination rate. If recombination occurs too fast (<0.1 ns), then there is not enough time for any other chemical reactions to occur.[1] In titania, the species are relatively long-lived (around 250 ns), allowing the electron or hole to travel to the crystallite surface. It is on the TiO_2 surface that different types of radicals are formed. The most common is the OH radical, which is then free to carry out further chemical reaction at the titania surface.[15]

To reduce recombination of photogenerated electrons and holes, and to extend its light absorption into the visible region, various transition metal cations have

* To whom correspondence should be addressed. Fax: (852) 2603-5057. E-mail: jimyu@cuhk.edu.hk.
† The Chinese University of Hong Kong.
‡ Wuhan University of Technology.

(1) Hoffmann, M. R.; Martin, S. T.; Choi, W.; Bahnemann, D. W. *Chem. Rev.* **1995**, *95*, 69.
(2) Fujishima, A.; Rao, T. N.; Tryk, D. A. *J. Photochem. Photobiol. C: Photochem. Rev.* **2000**, *1*, 1.
(3) Linsebigler, A. L.; Lu, G.; Yates, J. T. *Chem. Rev.* **1995**, *95*, 735.
(4) Tada, H.; Yamamoto, M.; Ito, S. *Langmuir* **1999**, *15*, 3699.
(5) Hattori, A.; Yamamoto, M.; Tada, H.; Ito, S. *Chem. Lett.* **1998**, 707.
(6) Asahi, R.; Morikawa, T.; Okwaki, T.; Aoki, K.; Taga, Y. *Science* **2001**, *293*, 269.
(7) Hu, C.; Wang, Y. Z.; Tang, H. X. *Appl. Catal. B: Environ.* **2001**, *30*, 277.
(8) Hu, C.; Wang, Y. Z.; Tang, H. X. *Chemosphere* **2000**, *41*, 1205.
(9) Yu, J. C.; Yu, J. G.; Zhao, J. C. *Appl. Catal. B: Environ.* **2002**, *36*, 31.
(10) Zhang, Q. H.; Gao, L.; Guo, J. K. *Appl. Catal. B: Environ.* **2000**, *26*, 207.
(11) Fox, M. A.; Dulay, M. T. *Chem. Rev.* **1993**, *93*, 341.
(12) Fujihira, M.; Satoh, Y.; Osa, T. *Nature* **1981**, *293*, 206.
(13) Hotsenpiller, P. A. M.; Bolt, J. D.; Farneth, W. E.; Lowekamp, J. B.; Rohrer, G. S. *J. Phys. Chem. B* **1998**, *102*, 3216.
(14) Gruy, F.; Pijolat, M. *J. Am. Ceram. Soc.* **1992**, *75*, 657.
(15) Ovenstone, J. *J. Mater. Sci.* **2001**, *36*, 1325.
(16) Yu, J. G.; Zhao, X. J.; Du, J. C.; Chen, W. M. *J. Sol−Gel Sci. Technol.* **2000**, *17*, 163.

10.1021/cm020027c CCC: $22.00
Published on Web 08/13/2002

been doped into titania.[17−22] For example, Choi et al.[19] conducted a systematic study of metal ion doping in quantum (Q)-sized TiO_2 for 21 metal ions. They found that doping with Fe^{3+}, Mo^{5+}, Ru^{3+}, Os^{3+}, Re^{5+}, V^{4+}, and Rh^{3+} at 0.1−0.5 at. % significantly increased the photoreactivity for both oxidation and reduction, while Co^{3+} and Al^{3+} doping decreased the photoreactivity for carbon tetrachloride reduction and chloroform oxidation. The photoreactivity of doped TiO_2 appeared to be a complex function of the dopant concentration, the energy level of dopant within the TiO_2 lattice, their d electronic configuration, the distribution of dopants, the electron donor concentration, and the light intensity. Doping of anions has also been investigated. Wang and Mallouk[23,24] published a study about the photocatalytic fluorination of organic molecules on the surface of titanium dioxide by adsorption of fluoride and hydrofluoric acid. Okazaki and Shinoda reported that the photocatalytic activity of TiO_2 decreased with surface fluorination using fluoromathane.[25] Hattori et al.[5,26] found a significant enhancement on photocatalytic activity of TiO_2 powders or thin films by doping with F^- ions, and the mechanisms of photoactive enhancement were ascribed to the increase in the anatase crystallinity induced by F^- ions. Very recently, Asahi et al. reported that the photocatalytic activity and hydrophilicity of TiO_2 could be enhanced by nitrogen doped into the substitutional sites of TiO_2 ($TiO_{2-x}N_x$).[6] However, to our knowledge, the effects of F^- doping and heat treatment on photocatalytic activity and microstructures of nanocrystalline TiO_2 powders prepared by the sol−gel method using titanium tetraisopropoxide as the titanium source have not been reported. This work may provide new insights and understanding on the mechanisms of photoactivity enhancement by F^- doping into the lattice of TiO_2.

2. Experimental Section

2.1. Preparation. All chemicals used in this study were reagent-grade supplied from Aldrich and were used as received. Millipore water was used in all experiments.

Titanium tetraisopropoxide (TTIP) was used as a titanium source. NH_4F was used as a precursor of the dopant. NH_4F was dissolved in pure water and then TTIP (0.0125 mol) was added dropwise to 100 mL of the H_2O-NH_4F mixed solution under vigorous stirring at room temperature. The atomic ratios of F to Ti, which hereafter was designated as R_F, were 0, 0.5, 1, 3, 5, 10, and 20 nominal atomic % (at. %). Sol samples obtained by the hydrolysis process were aged in a closed beaker at room temperature for 24 h uto further hydrolyze the TTIP and obtain monodisperse TiO_2 particles. After aging, these samples were dried at 100 °C for about 8 h in air to vaporize water and alcohol in the gels and then ground to fine powders to obtain xerogel samples. The xerogel samples were calcined at temperatures of 400, 500, 600, and 700 °C in air for 1 h, respectively.

2.2. Characterization. The X-ray diffraction (XRD) patterns obtained on a Philips MPD 18801 X-ray diffractometer using Cu Kα radiation at a scan rate of 0.05° 2θ S^{-1} were used to determine the crystallite size and identity. The accelerating voltage and the applied current were 35 kV and 20 mA, respectively. The phase content of a sample was calculated from the integrated intensities of anatase (101), rutile (110), and brookite (121) peaks according to the literature.[27] The average crystallite sizes of anatase, rutile, and brookite were determined according to the Scherrer equation using the fwhm data of each phase after correcting the instrumental broadening.[27]

Normally, the anatase phase of titania is the main product in hydrolytic sol−gel synthesis of nanocrystalline titania. However, brookite is often present as a byproduct. Brookite can be detected by the appearance of its (121) peak at 2θ = 30.8° in powder X-ray diffraction (XRD) patterns. Interestingly, the existence of this brookite phase was overlooked in many previous studies.[28,29] Even if the intensity of the brookite (121) peak is very low compared to the anatase (101) peak, the amount of brookite may be considerable.[27,30]

The crystallization behavior was also monitored using a TG-DTA instrument (Setaram TG-DTA 92−16, France). Crystallite sizes and shapes were observed using transmission electron microscopy (TEM) (JEOL 1200EX, Japan). UV−vis absorption spectra of TiO_2 powders were obtained for the dry-pressed disk samples using a UV−visible spectrophotometer (Cary 100 Scan Spectrophotometers, Varian, U.S.A.). Absorption spectra were referenced to $BaSO_4$. To investigate the recombination and lifespan of photogenerated electrons/holes in the photocatalysts, the photoluminescence (PL) emission spectra of the samples were measured in the following procedure. Each sample was dry-pressed into a 10-mm-diameter round disk containing about 200 mg of mass. The sample disks were illuminated with a 10-mW and 325-nm He−Cd laser at ambient temperature. Then, the photoluminescence from the samples was collected and focused into a spectrometer (Spex1702) and detected by a Hamamatsu R943 photomultiplier tube (PMT). Finally, the signal from the PMT was sent into a lock-in amplifier before being recorded by a computer. X-ray photoelectron spectroscopy (XPS) measurements were done with a PHI Quantum 2000 XPS System with a monochromatic Al Kα source and a charge neutralizer; all the binding energies were referenced to the C 1s peak at 284.8 eV of the surface adventitious carbon. The Brunauer−Emmett−Teller (BET) surface area (S_{BET}) and pore size distribution were determined using a Micromeritics ASAP 2000 nitrogen adsorption apparatus. All the samples were degassed at 180 °C prior to BET measurements.

2.3. Photoactivity Measurement. Acetone (CH_3COCH_3) is a common chemical that is used extensively in a variety of industrial and domestic applications. Therefore, we chose it as a model contaminate chemical. Photocatalytic oxidation of acetone is based on the following reaction:[9,21,31,32]

$$CH_3COCH_3 + 4O_2 \rightarrow 3CO_2 + 3H_2O \qquad (1)$$

The photocatalytic activity experiments on F^--doped and undoped TiO_2 powders for the oxidation decomposition of

(17) Akubuiro, E. C.; Verykios, X. E. *J. Phys. Chem. Solids* **1989**, *50*, 17.
(18) Soria, J.; Conesa, J. C.; Augugliaro, V.; Schiarello, M.; Sclafani, A. *J. Phys. Chem.* **1991**, *95*, 274.
(19) Choi, W.; Termin, A.; Hoffmann, M. R. *J. Phys. Chem.* **1994**, *98*, 13669.
(20) Moon, J.; Takagi, H.; Fujishiro, Y.; Awano, M. *J. Mater. Sci.* **2001**, *36*, 949.
(21) Lin, J.; Yu, J. C.; Lo, D.; Lam, S. K. *J. Catal.* **1999**, *183*, 368.
(22) Yuan, Z. H.; Jia, J. H.; Zhang, L. D. *Mater. Chem. Phys.* **2002**, *73*, 323.
(23) Wang, C. M.; Mallouk, T. E. *J. Phys. Chem.* **1990**, *94*, 4276.
(24) Wang, C. M.; Mallouk, T. E. *J. Am. Chem. Soc.* **1990**, *112*, 2016.
(25) Okazaki, S.; Shinoda, K. *J. Jpn. Soc. Colour Mater.* **1990**, *63*, 750.
(26) Hattori, A.; Shimoda, K.; Tada, H.; Ito, S. *Langmuir* **1999**, *15*, 5422.
(27) Zhang, H.; Banfield, J. F. *J. Phys. Chem. B* **2000**, *104*, 3481.
(28) Kumar, K. N. P.; Keizer, K.; Burggraaf, A. J. *J. Mater. Chem.* **1993**, *3*, 1141.
(29) Lin, Y. S.; Chang, C. H.; Gopalan, R. *Ind. Eng. Chem. Res.* **1994**, *33*, 860.
(30) Zhang, H.; Finnegan, M.; Banfield, J. F. *Nano Lett.* **2001**, *1*, 81.
(31) Zorn, M. E.; Tompkins, D. T.; Zeltner, W. A.; Anderson, M. A. *Appl. Catal. B: Environ.* **1999**, *23*, 1.
(32) Fernandez, A.; Lassaletta, G.; Jimenez, V. M.; Justo, A.; Gonzalez-Elipe, A. R.; Herrmann, J. M.; Tahiri, H.; Ait-Ichou, Y. *Appl. Catal. B: Environ.* **1995**, *7*, 49.

acetone in air were performed at ambient temperature using a 7000-mL reactor. The photocatalysts were prepared by coating an aqueous suspension of TiO_2 powders onto three dishes with diameters of 7.0 cm. The weight of the photocatalyst used for each experiment was kept at about 0.3 g. The TiO_2 photocatalysts were dried in an oven at 100 °C for about 2 h and then cooled to room temperature before use. After the dishes coated with TiO_2 powder photocatalysts were placed in the reactor, a small amount of acetone was injected into the reactor. The reactor was connected to a dryer containing $CaCl_2$ that was used for controlling the initial humidity in the reactor. The analysis of acetone, carbon dioxide, and water vapor concentration in the reactor was on line conducted with a Photoacoustic IR Multigas Monitor (INNOVA Air Tech Instruments Model 1312).[9,21] The acetone vapor was allowed to reach adsorption equilibrium with the catalyst in the reactor prior to an experiment. The initial concentration of acetone after the adsorption equilibrium was about 400 ppm, which remained constant until a 15-W, 365-nm UV lamp (Cole-Parmer Instrument Co.) in the reactor was switched on. Integrated UV intensity in the range 310−400 nm striking the films measured with a UV radiometer (UVX, UVP Inc., California, U.S.A.) was 540 ± 10 μW/cm^2, while the peak wavelength of UV light is 365 nm. The initial concentration of water vapor was 1.20 ± 0.01 vol %, and the initial temperature was 25 ± 1 °C. During the photocatalytic reaction, a near 3:1 ratio of carbon dioxide products to acetone destroyed was observed, and the acetone concentration decreased steadily with an increase in UV illumination time. Each reaction was followed for 60 min.

The photocatalytic activity of the films can be quantitatively evaluated by comparing the apparent reaction rate constants. The photocatalytic degradation generally follows a Langmuir−Hinshelwood mechanism[1,2,9,32] with the rate r being proportional to the coverage θ,

$$r = k\theta = kKc/(1 + Kc) \quad (2)$$

where k is the true rate constant which includes various parameters such as the mass of catalyst, the intensity of light, etc., and K is the adsorption constant. Since the initial concentration is low (c_o = 400 ppm = 4.29 × 10^{-3} mol/L), the term Kc in the denominator can be neglected with respect to unity and the rate becomes, apparently, first order,

$$r = -\,\mathrm{d}c/\mathrm{d}t = kKc = k_a c \quad (3)$$

where k_a is the apparent rate constant of pseudo-first-order. The integral form $c = f(t)$ of the rate equation is

$$\ln c_o/c = k_a t \quad (4)$$

The photocatalytic behavior of Degussa P-25 (P25) was also measured as a reference to compare with that of the synthesized catalysts. The measurements were repeated for each catalytic system, and the experimental error was found to be within ±5%.

3. Results and Discussion

3.1. Thermal Analysis. Figure 1 shows differential thermal analysis-thermogravimetry (DTA-TG) curves of TiO_2 xerogel powders prepared from the H_2O-NH_4F mixed solution with R_F = 1 and dried at 100 °C for 8 h. A broad endothermic peak exists at around 100 °C due to the desorption of water and alcohol. The relatively small exothermic peak at 261 °C comes from the decomposition of organic substances contained in the xerogel.[33,34] At about 400 °C, a small exothermic peak is observed due to further crystallization or formation of anatase phase.[33,34] The DTA curve also shows two relatively small exothermic peaks at about 697 and 605 °C. These are probably caused by the phase transitions

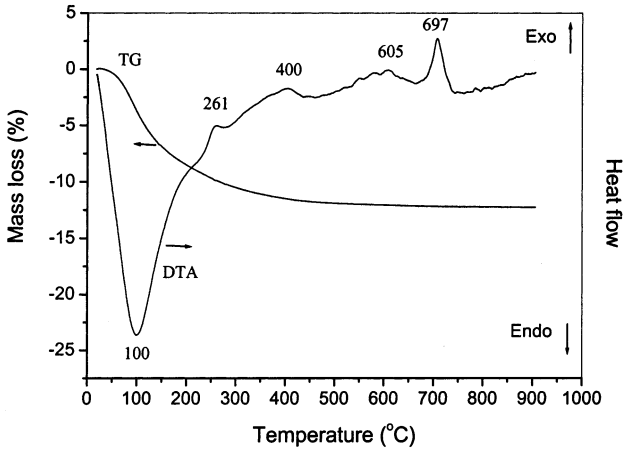

Figure 1. DTA-TG curves of TiO_2 xerogel powders prepared from the H_2O-NH_4F mixed solutions with R_F = 1 and dried at 100 °C for 8 h.

Table 1. Effects of Calcination Temperature and R_F on Phase Structure, Average Crystalline Size (nm), and Relative Anatase Crystallinity (Indicated in Parentheses) of TiO_2[a]

R_F	100 °C, 8 h	400 °C, 1 h	500 °C, 1 h	600 °C, 1 h	700 °C, 1 h
0	A: 5.8 (1) B: 3.1	A: 6.9 (1.35) B: 6.6	A: 9.3 (2) B: 6.8	A: 21.2 (3.7) R: 40.4 B: 18.3	A: 41.3 (0.2) R: 55.8
1	A: 5.7 (0.95) B: 4.8	A: 8.5 (1.5) B: 6.3	A: 12.6 (2.4) B: 6.5	A: 23.3 (3.7) R: 15.0 B: 25.9	A: 37.4 (0.2) R: 57.8
5	A: 5.7 (1.1) B: 4.7	A: 11.4 (2) B: 8.4	A: 13.9 (2.6) B: 9.3	A: 18.5 (3.3) B: 11.4	A: 32.9 (5.1) R: 52.2 B: 26.7
10	A: 4.3 (0.8)	A: 11.9 (2.1)	A: 17.5 (3.3)	A: 19.6 (4.0)	A: 24.8 (4.9)
20	A: 4.3 (0.9)	A: 12.6 (2.6)	A: 17.9 (3.4)	A: 21.2 (4.2)	A: 26.4 (5.0)

[a] A, B, and R denote anatase, brookite, and rutile, respectively. The average crystalline size of TiO_2 was determined by XRD using the Scherrer equation. Relative anatase crystallinity: the relative intensity of the diffraction peak from the anatase (101) plane (indicated in parentheses, reference = sample prepared from R_F = 0 and dried at 100 °C).

from anatase to rutile or brookite to rutile.[35] With increasing R_F, the exothermic peak position of rutile phase formation shifts to a much higher temperature range. This indicates that the phase transformation of anatase to rutile is suppressed by the presence of F^- ions (as shown in Tables 1 and 2). The TG curve can be divided into three stages. The first stage is from room temperature to 200 °C, over which the mass loss is the greatest. A mass loss of up to 8.8% was observed, which was caused by dehydration and evaporation of alcohol from the xerogels. The second stage is from 200 to 400 °C, where the mass loss is ≈2.5%. This can be assigned to the combustion and carbonization of most organic contents in the xerogels. The third stage is from 400 to 650 °C, where the mass loss is about 0.9%. This is attributed to the oxidation of carbon residue and evaporation of chemisorbed water.[34]

3.2. Crystal Structure. XRD was used to investigate the changes of phase structure of the as-prepared TiO_2 xerogel powders before and after heat treatment. Figure 2 shows the effects of R_F on phase structures of the TiO_2

(33) Terabe, K.; Kato, K.; Miyazaki, H.; Yamaguchi, S.; Imai, A.; Iguchi, Y. *J. Mater. Sci.* **1994**, *29*, 1617.
(34) Yu, J. G.; Zhao, X. J.; Zhao, Q. N. *Thin Solid Films* **2000**, *379*, 7.
(35) Yu, J. C.; Yu, J. G.; Ho, W. K.; Zhang, L. Z. *Chem. Commun.* **2001**, 1942.

Table 2. Effects of Calcination Temperature and R_F on Phase Content (%) of TiO_2[a]

R_F	100 °C, 8 h	400 °C, 1 h	500 °C, 1 h	600 °C, 1 h	700 °C, 1 h
0	A: 64.7	A: 65.3	A: 73.5	A: 79.1	A: 5.6
	B: 35.3	B: 34.7	B: 26.5	B: 14.0	B: 0
				R: 6.9	R: 94.4
1	A: 66.9	A: 69.9	A: 75.8	A: 72.	A: 7.8
	B: 33.1	B: 30.1	B: 24.2	B: 22.3	B: 0
				R: 5.7	R: 92.2
5	A: 71.5	A: 73.5	A: 76.1	A: 78.1	A: 74.5
	B: 28.5	B: 26.5	B: 23.9	B: 21.9	B: 9.0
					R: 16.5
10	A: 100	A: 100	A: 100	A: 100	A: 100
20	A: 100	A: 100	A: 100	A: 100	A: 100

[a] A, B, and R denote anatase, brookite, and rutile, respectively.

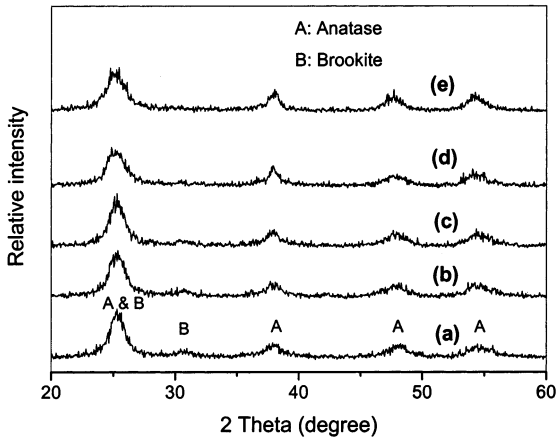

Figure 2. XRD patterns of the TiO_2 xerogel powders prepared from the H_2O-NH_4F mixed solution with $R_F = 0$ (pure water) (a), 1 (b), 5 (c), 10 (d), and 20 (e) and dried at 100 °C for 8 h.

xerogel powders prepared from the H_2O-NH_4F mixed solution and dried at 100 °C for 8 h. The anatase phase is dominant in the as-prepared TiO_2 xerogel powder from pure water ($R_F = 0$), but there is a small amount of brookite in it. The small peak at $2\theta = 30.7°$ corresponds to the brookite phase of titania. The presence of this phase causes the slight shift to a higher angle of the anatase peak since there is an overlapping brookite peak. With increasing R_F, the intensities of brookite peaks steadily become weaker and finally disappear when $R_F \geq 10$. This is probably due to the fact that F^- ions suppress the crystallization of brookite by adsorbing on to the surfaces of TiO_2 particles. An alternative explanation is that F^- ions catalyze the brookite to anatase transformation.

Figure 3 shows the effects of calcination temperature on phase structures of F^--doped TiO_2 powders prepared from the H_2O-NH_4F mixed solution with $R_F = 1$. It can be seen that, with increasing calcination temperature (From 400 to 600 °C), the peak intensities of anatase increase and the width of the (101) plane diffraction peak of anatase ($2\theta = 25.4°$) becomes narrower. The rutile phase starts to appear at 600 °C. TiO_2 powders thus contain three different phases: anatase, brookite, snd rutile. At 700 °C, rutile is a main phase and brookite disappears. Figure 4 shows XRD patterns of TiO_2 powders prepared from the H_2O-NH_4F mixed solution with $R_F = 20$ and calcined at different temperatures. The resulting TiO_2 powders contain only anatase phase over the calcination temperature range of 400−700 °C.

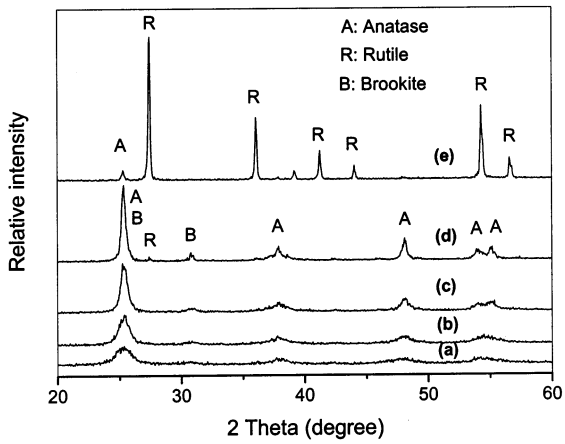

Figure 3. XRD patterns of TiO_2 powders prepared from the H_2O-NH_4F mixed solution with $R_F = 1$ and calcined at (a) 100, (b) 400, (c) 500, (d) 600, and (e) 700 °C for 1 h.

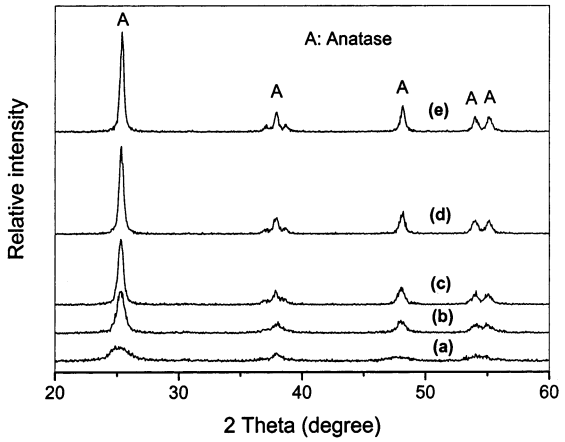

Figure 4. XRD patterns of TiO_2 powders prepared from the H_2O-NH_4F mixed solution with $R_F = 20$ and calcined at (a) 100, (b) 400, (c) 500, (d) 600, and (e) 700 °C for 1 h.

Table 1 shows the average crystalline size and relative anatase crystallinity of TiO_2 samples as a function of calcination temperature and R_F. At temperatures lower than 500 °C ($R_F = 0$ or 1) or 600 °C ($R_F = 5$), anatase and brookite phases are present in relatively small grain sizes. However, at 600 °C ($R_F = 0$ or 1) or 700 °C ($R_F = 5$), anatase, brookite, and rutile phases are all present and the grains of various phases grow dramatically. This is attributable to the fact that the phase transitions accelerate the process of grain growth by providing the heat of phase transformation.[35−37] At 700 °C, when $R_F \leq 1$, the relative anatase crystallinity significantly decreases due to the formation of a large amount of rutile as shown in Table 2. Table 2 also shows the effect of calcination temperature and R_F on the brookite content of TiO_2. In the temperature range lower than 500 °C ($R_F = 0$ or 1) or 600 °C ($R_F = 5$), the brookite content slightly decreases with increasing calcination temperature. As there is a corresponding increase in the anatase content. it can be concluded that brookite is gradually converted to anatase over this temperature range. At a temperature of 700 °C ($R_F = 0$ or 1), the brookite disappears. The rutile is dominant and there

(36) Yu, J. C.; Yu, J. G.; Zhang, L. Z.; Ho, W. K. *J. Photochem. Photobiol. A. Chem.* **2002**, *148*, 265.
(37) Ye, X.; Sha, J.; Jiao, Z.; Zhang, L. *Nanostruct. Mater.* **1997**, *7*, 919.

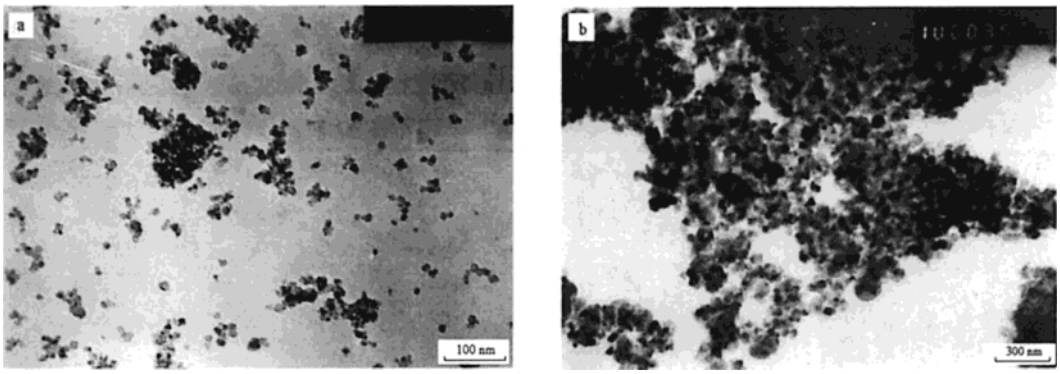

Figure 5. TEM photographs of TiO_2 powders prepared by hydrolysis of TTIP in the H_2O-NH_4F mixed solution with $R_F = 1$ and calcined at (a) 500 and (b) 700 °C for 1 h.

is only a trace of anatase. It can also be seen from Tables 1 and 2 that, at 400 and 500 °C, with increasing R_F, the crystallite sizes, content, and relative crystallinity of anatase increase. This is because the crystallinity of anatase is improved upon F^- doping.[5,26,38] It is interesting to note that, at temperatures below 600 °C, the brookite composition decreases with increasing R_F. This phase disappears completely at $R_F \geq 10$. A similar trend can also be observed for the rutile phase. At 700 °C, the rutile composition decreases with increasing R_F, and it is completely gone at $R_F \geq 10$. Hence, we believe that the F^- ions not only suppress the formation of brookite but also prevent phase transition of anatase to rutile. Our results also suggest the possibility of direct phase transformation from brookite to rutile without going through the anatase phase.[37]

Figure 5 shows TEM photographs of TiO_2 powders prepared by hydrolysis of TTIP in the H_2O-NH_4F mixed solution with $R_F = 1$ and calcined at (a) 500 and (b) 700 °C for 1 h. At 500 °C, the size of the primary particle is about 12 ± 2 nm, which is in agreement with the value determined by XRD (12.6 nm). At 700 °C, some of the particles are fused together through sintering, which explains the significant decrease in S_{BET} with increasing calcination temperature.

3.3. BET Surface Areas and Pore Structure. Figure 6 shows the pore size distribution curve calculated from the desorption branch of the nitrogen isotherm by the BJH method and the corresponding nitrogen adsorption−desorption isotherms (inset) of TiO_2 powders prepared from the mixed solution of H_2O-NH_4F with $R_F = 1$ and calcined at 500 °C for 1 h. The sharp decline in desorption curve is indicative of mesoporosity, while the hysteresis between the two curves demonstrates that there is a diffusion bottleneck, possibly caused by nonuniform pore size. The pore size distribution calculated from the desorption branch of the nitrogen isotherm by the BJH (Barrett−Joyner−Halenda) method shows a narrow range of 4.0−11.0 nm with an average pore diameter of ≈9.2 nm.

Table 3 shows that all samples prepared by our method have mesoporous structures. Such structures are the result of the pores formed between TiO_2 particles.[35,36,39] The diameters of mesopores are several to more than 20 nm. These mesopores allow rapid diffusion of various gaseous reactants and products during photocatalytic reaction and enhance the rate of photocatalytic reaction. It can be seen from Table 3 that when $R_F = 1$, the as-prepared TiO_2 xerogel powders dried at 100 °C for 8 h show a very large S_{BET} value of 270.9 $m^2 g^{-1}$. However, the surface area, porosity, and pore volume all become smaller with increasing calcination temperature. Meanwhile, the pore diameter increases

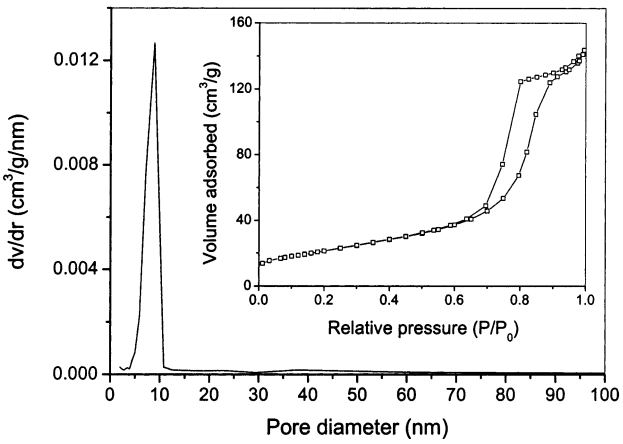

Figure 6. Pore size distribution curve calculated from the desorption branch of the nitrogen isotherm by the BJH method and the corresponding nitrogen adsorption−desorption isotherms (inset) of F^--doped TiO_2 powders prepared from the H_2O-NH_4F mixed solution with $R_F = 1$ and calcined at 500 °C for 1 h.

Table 3. Effect of Calcination Temperature and R_F on BET Surface Areas and Pore Parameters of TiO_2 Powders

R_F[a]	calcination temp. (°C)	S_{BET}[b] ($m^2 g^{-1}$)	porosity[c]	pore volume[d] (mL g^{-1})	pore size[e] (nm)
1	100	270.9	55.2	0.333	4.9
1	400	138.9	50.9	0.280	8.1
1	500	76.5	43.8	0.210	9.2
1	600	45.2	37.8	0.164	14.5
1	700	4.72	8.0	0.023	19.8
0	500	107.8	44.9	0.220	8.2
5	500	68.7	42.7	0.201	15.4
10	500	43.6	41.2	0.189	18.9
20	500	25.6	36.6	0.156	23.4

[a] The molar ratios of NH_4F to TiO_2. [b] BET surface area calculated from the linear part of the BET plot ($P/P_0 = 0.05-0.3$). [c] The porosity is estimated from the pore volume determined using the adsorption branch of the N_2 isotherm curve at about $P/P_0 = 0.975$ single point. [d] Total pore volume, taken from the volume of N_2 adsorbed at about $P/P_0 = 0.975$. [e] Average pore diameter, estimated using the adsorption branch of the isotherm and the Barrett−Joyner−Halenda (BJH) formula.

(38) Hattori, A.; Tada, H. *J. Sol−Gel Sci. Technol.* **2001**, *22*, 47.
(39) Huang, W.; Tang, X.; Wang, Y.; Koltypin, Y.; Gedanken, A. *Chem. Commun.* **2000**, 1415.

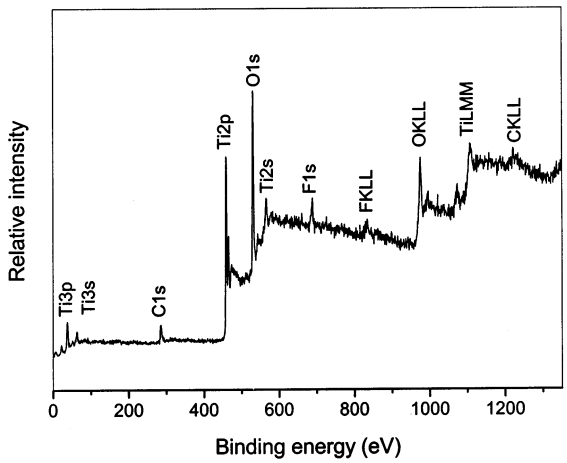

Figure 7. XPS survey spectrum of F⁻-doped TiO_2 powders prepared by hydrolysis of TTIP in the H_2O-NH_4F mixed solution with $R_F = 5$ and calcined at 500 °C for 1 h.

due to the growth of TiO_2 crystallites. Owing to sintering and phase transformation of anatase to rutile at 700 °C, the BET surface area of the same sample decreases drastically to 4.7 $m^2\ g^{-1}$. Table 3 also shows that, at 500 °C, when $R_F = 0$, the S_{BET} value of undoped TiO_2 is higher than that of F⁻-doped TiO_2. This is because the former has a smaller TiO_2 crystallite (9.3 nm). With increasing R_F, the S_{BET} value of F⁻-doped TiO_2 decreases steadily. This may be ascribed to the fact that the greater the amount of F⁻ ions in the TiO_2 xerogels, the stronger the promoting action of TiO_2 anatase crystallization. This would favor the formation of larger TiO_2 crystallites.

3.4. XPS Studies. Figure 7 shows the XPS survey spectrum of F⁻-doped TiO_2 powders prepared by hydrolysis of TTIP in the H_2O-NH_4F mixed solution with $R_F = 5$ and calcination at 500 °C for 1 h. XPS peaks show that the F⁻-doped TiO_2 powders contain only Ti, O, and F elements and a trace amount of carbon. The following binding energies are used in our quantitative measurements: Ti 2p at 458 eV, O 1s at 531 eV, F 1s at 688 eV, and C 1s at 284 eV. The atomic ratio of Ti:O:F is 1:2.13:0.06, which is in good agreement with the nominal atomic composition of TiO_2. The C element is ascribed to the residual carbon from precursor solution and the adventitious hydrocarbon from the XPS instrument itself. The XPS spectra of other samples are similar.

Figure 8 shows the high-resolution XPS spectra of the F 1s region, taken on the surface of the F⁻-doped TiO_2 powders prepared by hydrolysis of TTIP in the H_2O-NH_4F mixed solution with $R_F = 5$ and heat-treated at 100 (a) and 500 °C (b). The F 1s region is composed of two contributions. The main contribution is the F in solid solution $TiO_{2-x}F_x$, which is probably formed by nucleophilic substitution reaction of F⁻ ions and titanium alkoxide during the hydrolysis process.[23,40] The minor contribution is assigned to F⁻ ions physically adsorbed on the surface of TiO_2. Table 4 lists the results of curve fitting of F 1s XPS spectra. As indicated in Table 4 and Figure 8, the F content in solid solution $TiO_{2-x}F_x$ at 500 °C is higher than that at 100 °C. This

(40) Minero, C.; Mariella, G.; Maurino, V.; Vione, D.; Pelizzetti, E. *Langmuir* **2000**, *16*, 8964.

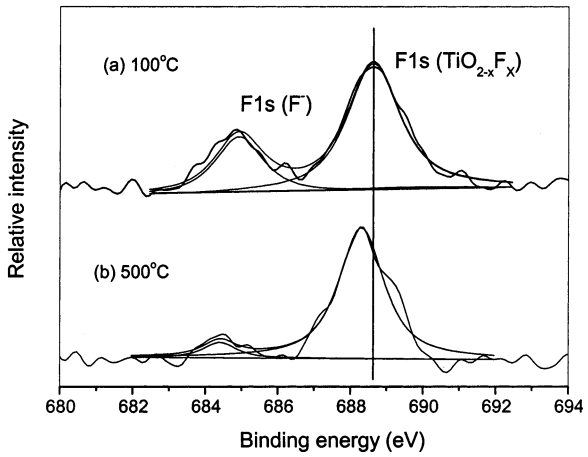

Figure 8. F 1s high-resolution XPS spectra of F⁻-doped TiO_2 powders prepared by hydrolysis of TTIP in the H_2O-NH_4F mixed solution with $R_F = 5$ and calcined at 100 (a) and 500 °C (b) for 1 h.

Table 4. Results of Curve Fitting of the High-Resolution XPS Spectra for the F 1s Region[a]

samples		F 1s (F^-)	F 1s ($TiO_{2-x}F_x$)
$TiO_{2-x}F_x$ at 100 °C	E_b (eV)	684.8	688.6
	r_i (%)	29.4	70.6
$TiO_{2-x}F_x$ at 500 °C	E_b (eV)	484.4	688.3
	r_i (%)	8.7	91.3

[a] r_i (%) represents the ratio $A_i/\Sigma A_i$ (A_i is the area of each peak). TiO_2 powders prepared from the H_2O-NH_4F mixed solution with $R_F = 5$.

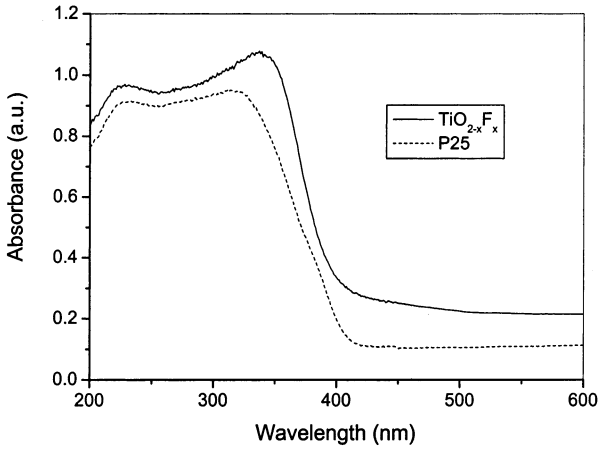

Figure 9. UV−visible absorption spectra of Degussa P-25 and the F⁻-doped TiO_2 powders prepared from the H_2O-NH_4F mixed solution with $R_F = 1$ and calcined at 500 °C for 1 h.

proves that thermal energy can trigger the substitution of F^- for O^{2-} in the lattice of TiO_2. In fact, the atomic radii of F^- and O^{2-} ions are about the same. It is not too surprising that nonstiochiometric solid solutions of $TiO_{2-x}F_x$ are formed.

3.5. Absorption Spectra. F⁻ doping obviously affects light absorption characteristics of TiO_2 as shown in Figure 9. A significant increase in the absorption at wavelengths shorter than 400 nm can be assigned to the intrinsic band gap absorption of pure anatase TiO_2 (≈3.2 eV). The absorption spectra of the F⁻-doped TiO_2 samples show a stronger absorption in the UV−visible range and a red shift in the band gap transition. Generally, the rate of the photocatalytic reaction is proportional to $(I_\alpha\phi)^n$ ($n = 1$ for low light intensity and

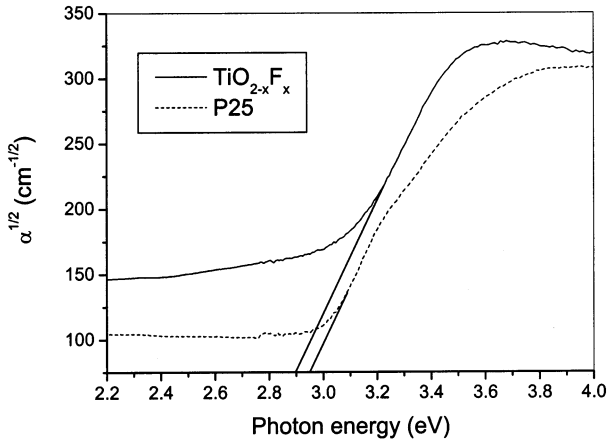

Figure 10. Plots of $(\alpha)^{1/2}$ versus photon energy ($h\nu$) for Degussa P-25 and the F^--doped TiO_2 powders prepared from the H_2O-NH_4F mixed solution with $R_F = 1$ and calcined at 500 °C for 1 h.

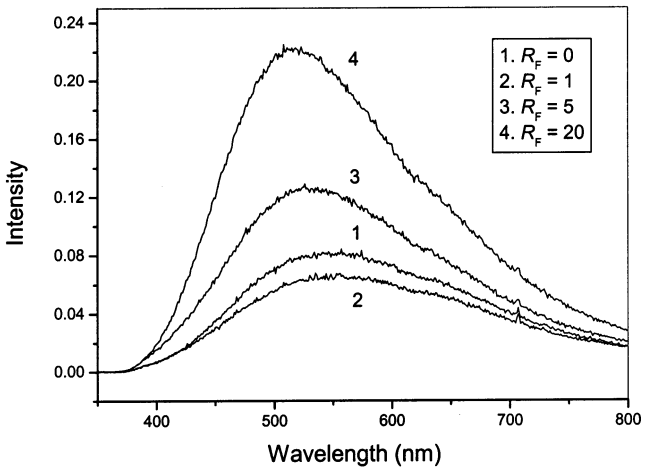

Figure 11. PL spectra of the F^--doped TiO_2 powders prepared from the H_2O-NH_4F mixed solution with $R_F = 0$ (pure water), 1, 5, and 20 and calcined at 500 °C for 1 h.

$n = 1/2$ for high light intensity), where I_α is the photo numbers absorbed by photocatalyst per second and ϕ is the efficiency of the band gap transition. The enhancement of the photoreactivity with F^- doping can be partly explained in terms of an increase in $I_\alpha\phi$ resulting from intensive absorbance in the UV region.[38] Moreover, F^- doping also expands the wavelength response range of TiO_2 to the visible region and increased the number of photogenerated electrons and holes to participate in the photocatalytic reaction. All these would enhance the photocatalytic activity of F^--doped TiO_2 powders.[6,41−42]

The absorption edge shifts toward longer wavelengths for the F^--doped TiO_2 powders. This clearly indicates a decrease in the band gap energy of TiO_2. Band gap energy can be estimated from a plot of $(\alpha)^{1/2}$ versus photon energy ($h\nu$). The intercept of the tangent to the plot will give a good approximation of the band gap energy for indirect band gap materials such as TiO_2.[43−45] The absorption coefficient α can be calculated from the measured absorbance (A) using the following equation,

$$\alpha = \frac{2.303\rho 10^3}{lcM}A \qquad (5)$$

where the density $\rho = 3.9$ g cm^{-3}, molecular weight $M = 79.9$ g mol^{-1}, c is the molar concentration of TiO_2, and l is the optical path length.[44]

Plots of $(\alpha)^{1/2}$ versus photon energy ($h\nu$) for P25 and the F^--doped TiO_2 powders are shown in Figure 10. The band gap energies are estimated to be 2.95 and 2.90 eV for P25 and the F^--doped TiO_2 powders, respectively. The finding that P25 has a lower band gap than the 3.2 eV of the bulk anatase is reasonable since P-25 consists of very fine particles with about 25% rutile content.[1,2] The red shift of the F^--doped TiO_2 powders is significant, as this sample is composed of both anatase and brookite phases ($R_F = 1$). It is known that the band gap energy of brookite should be higher than that of anatase.[46]

3.6. PL Spectra. Figure 11 shows the photoluminescence spectra for F^--doped and pure TiO_2. The difference of about 0.9 eV between the band gap energy (≈3.2 eV for anatase) and the emission peak energy (≈2.3 eV) is caused by the Stokes shift due to the Franck−Condon effect.[43] Close inspection of Figure 11 reveals a small shift of the emission peak toward the shorter wavelength as more fluoride ions are incorporated into TiO_2. This emission signal originates from the charge-transfer transition from Ti^{3+} to oxygen anion in a TiO_6^{8-} complex. Doping F^- ions creates slightly different environments in TiO_6^{8-}, and therefore the spectra of the doped and undoped TiO_2 are somewhat different.[47] The detailed mechanism is still being investigated. Figure 11 also shows a small decrease in emission intensity between sample 1 ($R_F = 0$) and sample 2 ($R_F = 1$). This indicates that an appropriate amount of F^- doping may slow the radiative recombination process of photogenerated electrons and holes in TiO_2. Samples with excessive F^- doping (samples 3 and 4), however, exhibit a significant increase in the emission intensity. This may be due to the introduction of new defect sites (or recombination centers) that enhances the recombination of photogenerated electrons and holes.[41,42] Our PL measurement results confirm that the higher the photocatalytic activity, the lower the intensity of PL spectra.

3.7. Photocatalytic Activity. Many studies have shown that calcination is an effective treatment method to enhance the photoactivity of nanosized TiO_2 photocatalysts.[10,48−51] Figure 12 shows the dependence of the apparent rate constants (k/min^{-1}) on calcination temperature. Samples of $R_F = 1$were prepared by hydrolysis of TTIP in a mixed solution of H_2O-NH_4F. The sample calcined at 100 °C shows decent photocatalytic activity

(41) Li, X. Z.; Li, F. B. *Environ. Sci. Technol.* **2001**, *35*, 2381.
(42) Li, X. Z.; Li, F. B.; Yang, C. L.; Ge, W. K. *J. Photochem. Photobiol. A: Chem.* **2001**, *141*, 209
(43) Rahman, M. M.; Krishna, K. M.; Soga, T.; Jimbo, T.; Umeno, M. *J. Phys. Chem. Solids* **1999**, *60*, 201.
(44) Kormann, C.; Bahnemann, D. W.; Hoffmann, M. R. *J. Phys. Chem.* **1988**, *92*, 5196.
(45) Yu, J. G.; Yu, J. C.; Ho, W. K.; Jiang, Z. T. *New J. Chem.* **2002**, *26*, 607.
(46) Mo, S. D.; Ching, W. Y. *Phys. Rev. B* **1995**, *51*, 13023.
(47) Fujihara, K.; Izumi, S.; Ohno, T.; Matsumura, M. *J. Photochem. Photobiol. A: Chem.* **2000**, *132*, 99.
(48) Kominami, H.; Murakami, S.; Kohno, M.; Kera, Y.; Okada, K.; Ohtani, B. *Phys. Chem. Chem. Phys.* **2001**, *3*, 4102.
(49) Tanaka, Y.; Suganuma, M. *J. Sol−Gel Sci. Technol.* **2001**, *22*, 83.
(50) Jung, K. Y.; Park, S. B. *Korean J. Chem. Eng.* **2001**, *18*, 879.
(51) Yu, J. C.; Lin, J.; Lo, D.; Lam, S. K. *Langmuir* **2000**, *16*, 7304.

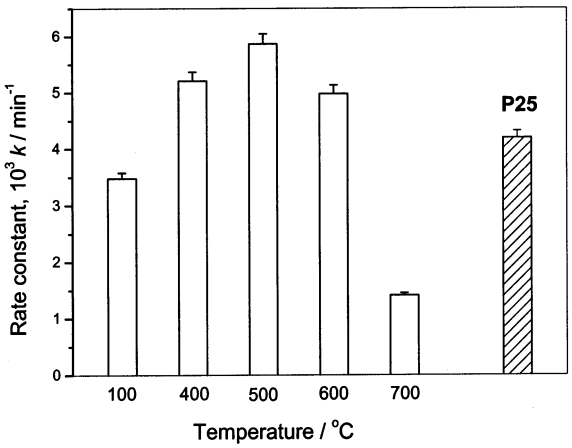

Figure 12. The dependence of the apparent rate constants (k/min^{-1}) on calcination temperature; all samples prepared by hydrolysis of TTIP in the H_2O-NH_4F mixed solution with $R_F = 1$.

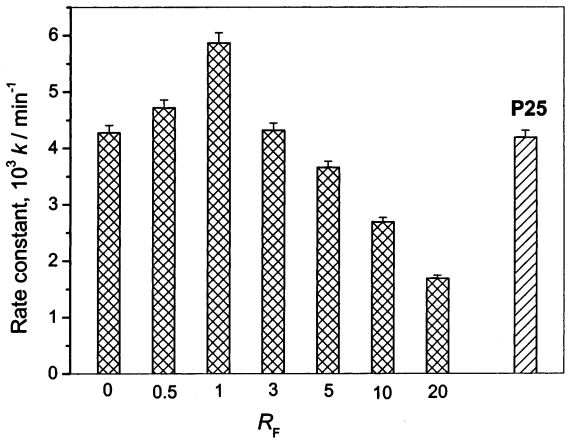

Figure 13. The dependence of the apparent rate constants (k/min^{-1}) on R_F; all samples prepared by hydrolysis of TTIP in the H_2O-NH_4F mixed solution and calcined at 500 °C for 1 h.

with a rate constant of 3.49×10^{-3}. The rate constant increases with increasing calcination temperature. The enhancement of photocatalytic activity at elevated temperatures can be ascribed to an obvious improvement in the crystallinity of anatase (as shown in Table 1). At a calcination temperature of 500 °C, the k reaches the highest value of 5.81×10^{-3}. This rate constant is even higher than that of P25 ($k = 4.19 \times 10^{-3}$), which is recognized as an excellent photocatalyst.[1,52] The high photocatalytic activity of the 500 °C sample is partially due to its large surface area and small crystallite size. Moreover, the intense absorption in the UV−visible range and a red shift in the band gap transition of the F^--doped TiO_2 samples are indications that more photogenerated electrons and holes can participate in the photocatalytic reactions. Similar results have been observed with nitrogen ion doping.[6,53] Calcination temperatures well above 500 °C are not desirable. Samples calcined at 700 °C display very poor photocatalytic activity. Treatment at such a high temperature would form TiO_2 powders that are composed of mostly rutile phase (as shown in Table 2) and have poor specific surface areas (as shown in Table 3).

Figure 13 shows the dependence of the apparent rate constants (k/min^{-1}) on R_F for samples calcined at 500 °C for 1 h. The k values increase with increasing R_F, and it peaks at $R_F = 1$. One possible explanation for this photocatalytic activity ehhancement is that F^- doping converts some Ti^{4+} to Ti^{3+} by charge compensation.[54]

$$(1-q)TiO_2 + qF^- \rightarrow Ti^{3+}_{\ q}Ti^{4+}_{\ 1-q}O^{2-}_{\ 2-q}F^-_{\ q} + q/2O^{2-} \quad (6)$$

Since TiO_2 is an n-type semiconductor, the Ti^{3+} surface states in TiO_2 form a donor level between the band gaps of TiO_2. The Ti^{3+} surface states may trap the photogenerated electrons and then transfer them to O_2 adsorbed on the surface of TiO_2. Therefore, the existence of a certain amount of Ti^{3+} surface states in TiO_2 results in the reduction of the electron and hole recombination rate and enhances photocatalytic activity.[55] Figure 14 shows the schematic energy level diagram for Ti^{3+} and charge-carrier dynamics in F^--doped TiO_2.[53,54] Upon UV excitation, photogenerated electrons accumulate at the lower lying surface state of Ti^{3+}, whereas holes accumulate at the valence band of TiO_2. Accumulated electrons at the surface state of Ti^{3+} can be transferred to oxygen adsorbed on the surface. This slows down the recombination of the electron−hole pairs. This effect is observed in samples with low dopant concentration ($R_F \leqslant 1$). Recently, Szczepankiewicz et al. reported direct FTIR evidence for electron and hole trapping by Ti(III) produced from a CB electron and >Ti(IV)OH· produced from a VB hole.[56] However, Ti^{3+} surface states produced by F doping may be different from Ti(III) produced from a CB electron during UV illumination because the former is caused by charge equilibrium. When the dopant concentration becomes too high ($R_F > 1$), the recombination rate will increase because the distance between trapping sites in a particle decreases with the number of dopants.[20] It should be noted that samples prepared from pure water or the H_2O-NH_4F mixed solutions with $R_F \leqslant 5$ and calcined at 500 °C are all composed of two phases, and they show good photoac-

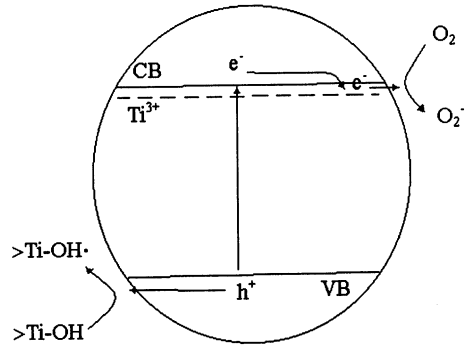

Figure 14. Schematic energy level diagram for Ti^{3+} and charge-carrier dynamics in F^--doped TiO_2.

(52) Piscopo, A.; Robert, D.; Weber, J. V. *J. Photochem. Photobiol. A: Chem.* **2001**, *139*, 253.
(53) Morikawa, T.; Asahi, R.; Okwaki, T.; Aoki, K.; Taga, Y. *Jpn. J. Appl. Phys. Lett.* **2000**, *132*, 99.
(54) Lin, H.; Kumon, S.; Kozuka, H.; Yoko, T. *Thin Solid Films* **1998**, *315*, 266.
(55) Yu, J. G.; Zhao, X. J.; Zhao, Q. N. *Mater. Chem. Phys.* **2001**, *69*, 25.
(56) Szczepankiewicz, S. H.; Colussi, A. J.; Hoffmann, M. R. *J. Phys. Chem.* **2000**, *104*, 9842.

tivity. Usually, the composite of two kinds of semiconductors or two phases of the same semiconductor is beneficial in reducing the recombination of photogenerated electrons and holes and thus enhances photocatalytic activity.[35] The interface between the two phases may act as a rapid separation site for the photogenerated electrons and holes due to the difference in the energy level of their conduction bands and valence bands. The samples prepared from $R_F \geqslant 10$ exhibit much lower photoactivity due to the absence of brookite phase.

The photochemical mechanism of vanadium-doped TiO_2 was investigated by Martin et al.[57] They found that V doping would reduce the photooxidation rates of 4-chlorophenol relative to undoped TiO_2, and an explanation based on the charge-carrier recombination by electron/hole trapping was proposed. Iron doping, on the other hand, generated very different results. A 40-fold enhancement on photoactivity with Fe(III) doping was reported by Choi et al.[19] As shown in Figure 12, the photocatalytic activity of our F^--doped TiO_2 is up to 39% higher than that of P25. This does not seem like much compared with the 40-fold improvement for Fe(III) doping. However, it should be noted that Choi et al. used a sample with low activity as a benchmark. Since P25 is considered an excellent photocatalyst, a 39% enhancement would be significant.

4. Conclusions

1. A simple method was developed for the preparation of highly photoactive nanocrystalline F^--doped TiO_2 photocatalysts with anatase and brookite phase by hydrolysis of titanium tetraisopropoxide in the NH_4F-H_2O mixed solution.

2. The crystallinity of anatase was improved upon F^- doping. Moreover, with increasing R_F, F^- ions not only suppressed the formation of brookite phase but also prevented phase transition of anatase to rutile.

3. The F^--doped TiO_2 samples showed stronger absorption in the UV−visible range and a red shift in the band gap transition.

4. At 500 °C, the photocatalytic activity of F^--doped TiO_2 powders prepared by this method with R_F in the range of 0.5−3 exceeded that of Degussa P25.

Acknowledgment. The work was partially supported by a grant from the National Natural Science Foundation of China and Research Grants Council of the Hong Kong Special Administrative Region, China (Project No. N_CUHK433/00). This work was also financially supported by the Foundation for University Key Teachers of the Ministry of Education and the National Natural Science Foundation of China (50072016). We are indebted to Prof. S. K. Hark and graduate student Kwan Sai Iu (Department of Physics, The Chinese University of Hong Kong) for acquiring the PL spectra. J. G. Yu expresses his sincere gratitude for the Postdoctoral Fellowships Scheme of The Chinese University of Hong Kong.

CM020027C

(57) Martin, S. T.; Morrison, C. L.; Hoffmann, M. R. *J. Phys. Chem.* **1994**, *98*, 13695.